Songklanakarin J. Sci. Technol.
41 (5), 1154-1161, Sep. – Oct. 2019

http://www.sjst.psu.ac.th

Original Article

Performance comparison between the ITER- and DEMO-like plasmas using CRONOS simulations

Boonyarit Chatthong[1*], and Jiraporn Promping[2]

[1] *Department of Physics, Faculty of Science, Prince of Songkla University, Hat Yai, Songkhla, 90112 Thailand*

[2] *Thailand Institute of Nuclear Technology, Chatuchak, Bangkok, 10900 Thailand*

Received: 21 March 2018; Revised: 15 June 2018; Accepted: 18 June 2018

Abstract

This work investigates plasma performance and fusion power production of the ITER- and DEMO-like plasmas using the integrated predictive modelling code CRONOS. These plasmas are simulated in the presence of an edge transport barrier (ETB). The transport effect includes both neoclassical and anomalous contributions. The neoclassical transport is described using the NCLASS module, while the anomalous transport is calculated using a semi-empirical Mixed Bohm/gyro-Bohm model. The boundary conditions for the transport equations are set at the top of the pedestal where the ETB forms. The pedestal height is calculated based on the scaling law. The time evolution of plasma current, temperatures, and density profiles of the ITER and DEMOs that include the Chinese, Japanese, Korean, Indian, and European designs, are simulated based on their engineering designs and conceptual plans. It was found that the European Model B yielded the highest temperatures and total fusion power. The ITER design generated high fusion Q, while both the ITER and Japanese DEMO yielded the longest energy confinement time. The highest bootstrap fraction was found in the Korean DEMO.

Keywords: plasma, tokamak, fusion, ITER, DEMO

1. Introduction

The future energy crisis remains an open issue. Fusion energy could play a big part providing the backbone energy for our ever-increasing energy demand. A magnetic confinement device, such as the tokamak experiment, has emerged as the leading approach for fusion research which has been actively investigated for over 50 years (Dale, 2010). During the 2020s, the multi-international project called the International Thermonuclear Experimental Reactor (ITER) will finish its construction and the first burning plasma experiment will begin. This is a collaboration project of seven partners including the European Union, China, Japan, South Korea, India, Russia, and the United States. Its aim is to demonstrate engineering and technological feasibilities of nuclear fusion (Aymar, Barabaschi, & Shimomura, 2002). The knowledge gained from the ITER experiments will be shared among the partners. Meanwhile, each of the ITER partners is developing its own DEMO program. The ITER is designed to be a fusion experimental machine while DEMO is designed to be a prototype nuclear fusion reactor.

High confinement mode (*H*-mode) is considered one of the major discoveries in fusion research (ASDEX Team, 1989; Wagner *et al.*, 1982). Historically, it was found that once either a limiter or a divertor was installed in the chamber and sufficient heating power was given to the plasma, the plasma could make an abrupt transition from low confinement mode (*L*-mode) to *H*-mode. As a result of this mode, the plasma temperature, density, and energy confinement time are significantly improved (Wagner, 2007). Because of this improvement, the ITER was redesigned to operate in *H*-mode (Aymar *et al.*, 2002). In addition, it is expected that the future DEMOs will also operate in *H*-mode. It is known that the plasma transits from *L*- to *H*-mode as a result of an edge

*Corresponding author
Email address: boonyarit.ch@psu.ac.th

transport barrier (ETB) formation (Hubbard, 2000). This is a narrow local region at the edge of the plasma where the plasma profile, including temperatures and densities, exhibit steep gradient values and that is the reason why that area is often called a pedestal. Theoretically, it is widely accepted that ETB formation is caused by high ω_{ExB} flow shear or radial electric field shear (Burrell, 1997), which results in suppression of turbulent or anomalous transport in the plasma.

The cost of construction and performing tokamak experiments can be rather expensive. The ITER cost is shared among the partners. The DEMOs could be even more expensive. Therefore, integrated predictive modelling codes are generally used to predict and develop plasma scenarios for the future experiments. Reliable codes can reduce the risk of machine damage and the actual experimental cost. Examples of widely used simulation codes are ASTRA (Pereverzev & Yushmanov, 2002), BALDUR (Singer *et al.*, 1988), CORSICA (Pearlstein *et al.*, 2001), CRONOS (Artaud *et al.*, 2010), JETTO (Cenacchi & Taroni, 1988), ONETWO (Deng *et al.*, 2009), TSC (Jardin, Pomphrey, & DeLucia, 1986), XPTOR (Kinsey, Staebler, & Waltz, 2002), and TASK (Honda & Fukuyama, 2008). Typically, they are transport solvers which compute for the spatiotemporal evolution of plasma current, ion temperatures, electron temperatures, impurities, densities, and magnetic equilibrium profiles. The input to the codes can be both physical and engineering parameters such as plasma geometry, heating type and power, external magnetic field, line average density, and plasma current. In the last ten years, numerous research projects have simulated the ITER performance based on a variety of scenarios such as full current, steady-state advanced scenario, and hybrid scenarios using these integrated predictive modelling codes (Basiuk *et al.*, 2003; Chatthong & Onjun, 2013; Chatthong & Onjun, 2014; Kessel *et al.*, 2007). On the other hand, integrated predictive codes were also used to prepare the DEMO campaigns (Feng *et al.*, 2009; Kim *et al.*, 2015; Maisonnier *et al.*, 2006; Srinivasan & Deshpande, 2008; Tobita *et al.*, 2006). These results were very important because they served as a basis recommendation for the construction of the devices.

In this paper, a CRONOS suite of codes, developed by Artaud *et al.* (2010) from CEA, France, is used to simulate and predict the time evolution profiles of ion temperatures, impurities, electron temperatures, electron density, and plasma current for the ITER- and DEMO-like plasmas. For the entire paper, simulations are solved based on current diffusion, electron and ion heat transport, and electron transport equations. The ion and impurity species are calculated based on the impurity module using the concept of charge neutrality in plasma and effective charge. The momentum transport equation in CRONOS has not yet been fully tested so it is ignored in this work. The transport effect combines neoclassical and anomalous transports. The ETB region follows a pedestal model based on an international scaling (Righi, 1998), which predicts the values at the top of the pedestal. These values are used as boundary conditions for the transport equations solver. The simulation results will compare plasma performance, i.e. ion and electron temperatures, electron density, fusion power, fusion Q, and confinement time. These factors will be evaluated to assess the best designs. Keep in mind that this study is based solely on the plasma physics point of view. Other factors such as engineering cost, feasibility, and economic evaluations are also needed in order to select the actual design. The results of this work serve as a comparison of the plasma products of each machine.

2. CRONOS Code

CRONOS is a 1.5D integrated predictive modelling code designed to solve the transport equation for various plasma quantities such as current density, electron and ion temperatures, ion densities, impurity species, toroidal momentum, and suprathermal particles (Artaud *et al.*, 2010). The transport equations are solved in 1D, which is the minor radius of a tokamak plasma representing a magnetic flux. CRONOS then solves for magnetic equilibrium, radiation and particle losses, and thermal and particle sources in 2D. The code is built in MATLAB and utilizes its graphical interface for user friendly handling. The code has been applied extensively to simulate and investigate plasma properties of the Tore Supra, ITER, and other tokamak devices (Basiuk *et al.*, 2003; Chouli *et al.*, 2015; Kessel *et al.*, 2007; Kim *et al.*, 2009). In this version of CRONOS, the current diffusion equation is employed to solve for the poloidal flux ψ surface. The current density is composed of two parts: inductive and non-inductive current density. The non-inductive current includes intrinsic bootstrap current and external driven currents by neutral beam injection (NBI), ion cyclotron waves, electron cyclotron waves, and lower hybrid (LH) waves. The details of its calculation can be seen in Artaud *et al.* (2010). In addition, CRONOS solves the electron heat transport equation which represents the conservation of electron thermal energy. It has the form (Hinton & Hazeltine, 1976):

$$\frac{3}{2}\frac{\partial}{\partial t}\left(p_e V^{\frac{5}{3}}\right)+V^{\frac{2}{3}}\frac{\partial}{\partial \rho}\left(V\left\langle|\nabla\rho|^2\right\rangle\left[q_e+\frac{5}{2}T_e\Gamma_e\right]\right)=V^{\frac{5}{3}}Q_e \quad (1)$$

where p_e is the electron pressure, V is the derivative of volume enclosed inside the magnetic flux surface, ρ is the flux surface radius, q_e is the electron heat flux, T_e is the electron temperature in keV, Γ_e is the electron particle flux and Q_e is the electron thermal source term, which consists of several effects such as electron-ion collisional exchange, neoclassical, ohmic, bremsstrahlung loss, and external heating sources. Similarly, the ion heat transport equation is in the form:

$$\frac{3}{2}\frac{\partial}{\partial t}\left(p_i V^{\frac{5}{3}}\right)+V^{\frac{2}{3}}\frac{\partial}{\partial \rho}\left(V\left\langle|\nabla\rho|^2\right\rangle\left[q_i+\frac{5}{2}T_i\Gamma_i\right]\right)=V^{\frac{5}{3}}Q_i \quad (2)$$

where p_i is the ion pressure of all ion species, q_i is the ion heat flux, T_i is the ion temperature in keV, which is assumed to be the same for all ion species, Γ_i is the ion particle flux and Q_i is the ion thermal source term.

As mentioned earlier, CRONOS only solves the particle transport equation for electron density. The ion densities, as well as those of impurities species, are calculated separately using an impurity module which is based on the charge neutrality of the plasma and effective charge Z_{eff} representing the average charge of the plasma. The electron particle transport equation has the form:

$$\frac{\partial}{\partial t}\left(n_e V\right)+\frac{\partial}{\partial \rho}\left(V\left\langle\left|\nabla\rho\right|^2\right\rangle\Gamma_e\right)=VS_e \tag{3}$$

where n_e is the electron density and S_e is the electron source term, which consists of neutrals ionization (at plasma edge), NBI, and particle loss contributions. The transport coefficients used for the calculation of the fluxes are a combination of the two effects, neoclassical and anomalous transports. The neoclassical transport is calculated by the well-known neoclassical transport (NCLASS) module (Houlberg, Shaing, Hirshman, & Zarnstorff, 1997). The anomalous transport, the dominant term, is calculated based on the semi-empirical mixed Bohm/gyro-Bohm transport model as discussed in more detailed in the next section.

2.1 Mixed Bohm/gyro-Bohm anomalous transport model

The anomalous transport, representing the turbulent effect, is modeled using a mixed Bohm/gyro-Bohm transport model. This model was initially developed based on Bohm scaling. Essentially, it is assumed that the diffusion coefficients are driven by plasma gyro-radius times thermal velocity. It was suitable to describe both electron and ion transport in a large tokamak device like JET (Erba, Parail, Springmann, & Taroni, 1995; Taroni, Erba, Springmann, & Tibone, 1994). Nevertheless, it was not so successful in calculating the transport for a small tokamak. Corrections were made using the gyro-Bohm contribution which assumes that the diffusion coefficients behave proportionally to the gyro-radius square times the thermal velocity divided by plasma major radius R (Erba, Aniel, Basiuk, Becoulet, & Litaudon, 1998). In mixed Bohm/gyro-Bohm, the transport coefficients used for flux calculations are computed as follows:

$$\chi_e = 0.07\chi_{gB}+\left(8\times10^{-5}\right)\chi_B \tag{4}$$

$$\chi_i = 0.0175\chi_{gB}+0.00016\chi_B \tag{5}$$

$$D_e = \left(0.3+0.7\rho\right)\frac{\chi_e\chi_i}{\chi_e+\chi_i} \tag{6}$$

$$\chi_{gB} = 5\times10^{-6}\sqrt{T_e}\left|\frac{\nabla T_e}{B_\phi^2}\right| \tag{7}$$

$$\chi_B = 4\times10^{-5}R\left|\frac{\nabla\left(p_e\right)}{n_eB_\phi^2}\right|q^2\left(\frac{T_e\left(0.8\rho_{\max}\right)-T_e\left(\rho_{\max}\right)}{T_e\left(\rho_{\max}\right)}\right) \tag{8}$$

where χ_e is the electron diffusivity, χ_i is the ion diffusivity, χ_{gB} is the gyro-Bohm diffusivity, χ_B is the Bohm diffusivity, D_e is the electron particle diffusivity, B_ϕ is the toroidal magnetic field, and q is the plasma safety factor. These coefficients are used to compute the electron heat flux, ion heat flux and electron particle flux using the simple forms of diffusive and convective combinations, respectively, as:

$$q_e = -\chi_e\frac{\partial T_e}{\partial\rho}-p_ev_e^q \tag{9}$$

$$q_e = -\chi_i\frac{\partial T_i}{\partial\rho}-p_iv_i^q \tag{10}$$

$$\Gamma_e = -D_e\frac{\partial n_e}{\partial\rho}-n_ev_e^\Gamma \tag{11}$$

where v_e^q, v_i^q, and v_e^Γ represent the pinch terms.

2.2 Pedestal model

The mechanism for an ETB formation is still unclear. Though, general fusion researchers accept that it is caused by the suppression of anomalous transport via decorrelation of turbulent convective cells (Burrell, 1997). This disruption of turbulent fluxes is believed to be a result of shear in the radial electric field or the ω_{ExB} flow shear. Nevertheless, the complete theory of *L*-*H* transition is not fully formulated yet. Therefore, in this work, the top of the pedestal is calculated based on an international multi-tokamak scaling data as follows (Snipes & Group, 2000):

$$T_{ped} = 141.69q_{95}^{-0.53}B_\phi^{0.99}R^{0.93}n_{ped}^{-0.13}\delta^{0.12} \tag{12}$$

where T_{ped} is the temperature at the pedestal, q_{95} is the safety factor at the last closed magnetic surface, δ is the plasma triangularity and n_{ped} is the density at the top of pedestal estimated empirically as:

$$n_{ped} = 0.65\bar{n}_e \tag{13}$$

with $\bar{n}_e$ is the electron line average density.

3. ITER and DEMO Setups

The tokamak ITER is in the construction phase in Cadarache, France and is expected to finish in the early 2020s. It will be the largest fusion device humans have ever created. The main goal of the ITER is to test engineering and technological feasibilities of a fusion reactor with expected 500 MW power output. The ITER is designed to produce a burning plasma, which means part of its heating will come from self-heating alpha particles. The ITER scenario used in this work is based on the standard type I ELMy *H*-mode using full current setup (Chatthong & Onjun, 2014).

DEMO, or demonstration power plant, is the next step after the ITER. Its goal in general is to test a steady-state fusion reactor. DEMO will produce its own tritium via tritium breeding process. The device itself will not be as complicated as the ITER because only the necessary diagnostic instruments will be installed. It will use the knowledge gained from the ITER experiment for a prototype power plant. While the ITER is being built, each of the ITER partners has already started

their own DEMO program. Several conceptual designs for DEMOs are being investigated in this work. The parameters used for simulations are taken from literature review of the Chinese DEMO (Feng *et al.,* 2009), Japanese DEMO (Tobita *et al.,* 2006), Korean DEMO (Kim *et al.,* 2015), Indian DEMO (Srinivasan & Deshpande, 2008), and European DEMO models A, B, C, and D (Maisonnier *et al.,* 2006). A summary of the engineering design parameters for the ITER and all DEMO devices are shown in Table 1. The abbreviation a represents plasma minor radius, I_P is the induced plasma current, κ is the plasma elongation which describes the shape of the cross-section of tokamak plasma, and P_{aux} is the total auxiliary heating power. In this work the heating power schemes consist of NBI, ion cyclotron range of frequency heating, and electron cyclotron range of frequency heating. Note that the European DEMO models A and B are designed to have higher plasma performance than the ITER at around 30% and models C and D are designed to optimize efficiency for reactor purposes.

Table 1. Summary of engineering design parameters for ITER and DEMOs.

Device	R (m)	a (m)	I_p (MA)	B_ϕ (T)	κ	δ	P_{aux} (MW)
ITER	6.2	2.0	15	5.3	1.7	0.33	40
Chinese	7.2	2.1	14.8	6.86	1.85	0.45	74
Japanese	5.5	2.1	16.7	6.0	2.0	0.4	59
Korean	6.8	2.1	12	7.4	2.0	0.625	80
Indian	7.7	2.6	17.8	6.0	1.7	0.33	125
EU A	9.55	3.18	30.5	7.0	1.7	0.25	246
EU B	8.6	2.87	28	6.9	1.7	0.25	270
EU C	7.5	2.5	20.1	6	1.9	0.47	112
EU D	6.1	2.03	14.1	5.6	1.9	0.47	71

4. Simulation Results

4.1 Temperature profiles

Examples of magnetic flux surface of the ITER and all DEMOs are shown as a cross-section in Figure 1. It can be seen that the main features are similar except the size and small shaping variation due to having different values of triangularity δ and elongation κ. The horizontal axis represents the major radius which is measured from the center of the device. The vertical axis represents the relative height of the plasma. This is a result from ITER simulation where the flux surface is calculated from the current density equation. Each magnetic flux surface goes around the donut-shaped tokamak toroidally. As plasma particles are free to move parallel to this surface, normally the plasma reaches equilibrium rather fast. For this reason, most transport code solves only in 1D, a radial direction. This can be seen in Figure 2 which shows ion temperature profiles as a function of normalized minor radius. The central ion temperature values are close to what is expected from a fusion reactor in the range of 40 keV. However, the European DEMO models A and B yield rather high ion temperatures. This is because these two designs are given with high external power and plasma current, which play roles in enhancing plasma temperatures. It can be observed that, for each profile, an ETB has formed at the edge of the plasma, r/a >0.9. One of the signatures of ETB region is a sudden steep gradient, illustrated at the bottom panels of Figure 2. Most of the results show a rather narrow ETB close to the edge except European DEMO models A and B. These profiles are possible because the simulations have not included gradient-limit instability. The ETB width can grow limitlessly as long as more heating power is given to the plasma. The mechanism of this kind of instability is still in

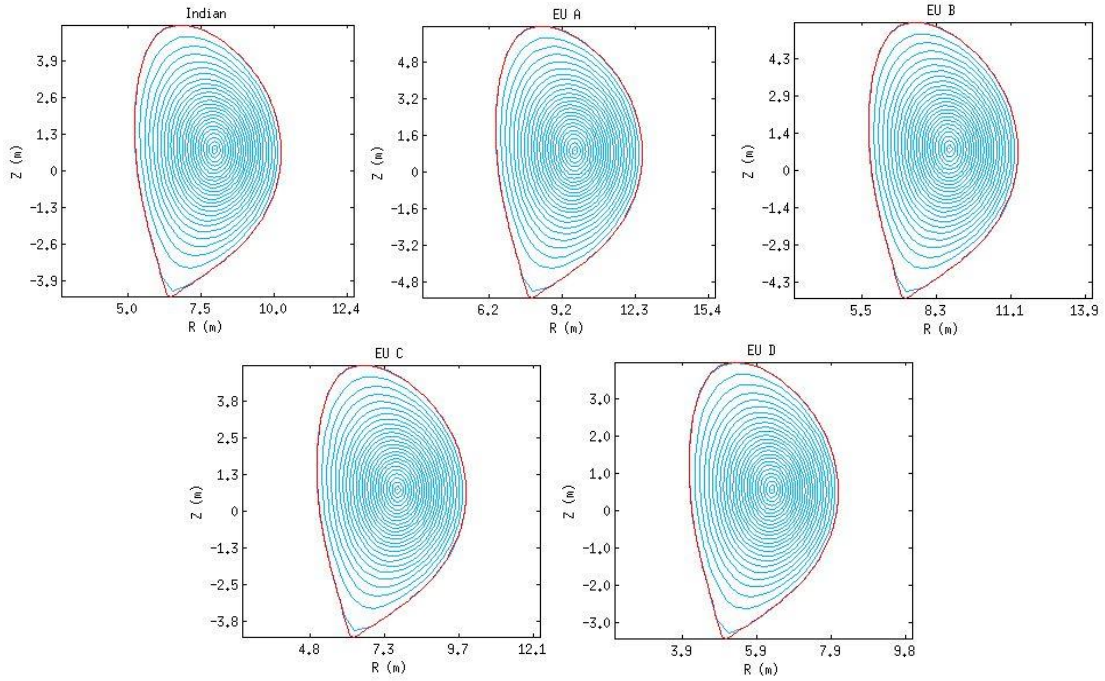

Figure 1. Equilibrium magnetic surface for the ITER and all DEMOs as a function of plasma major radius and vertical height.

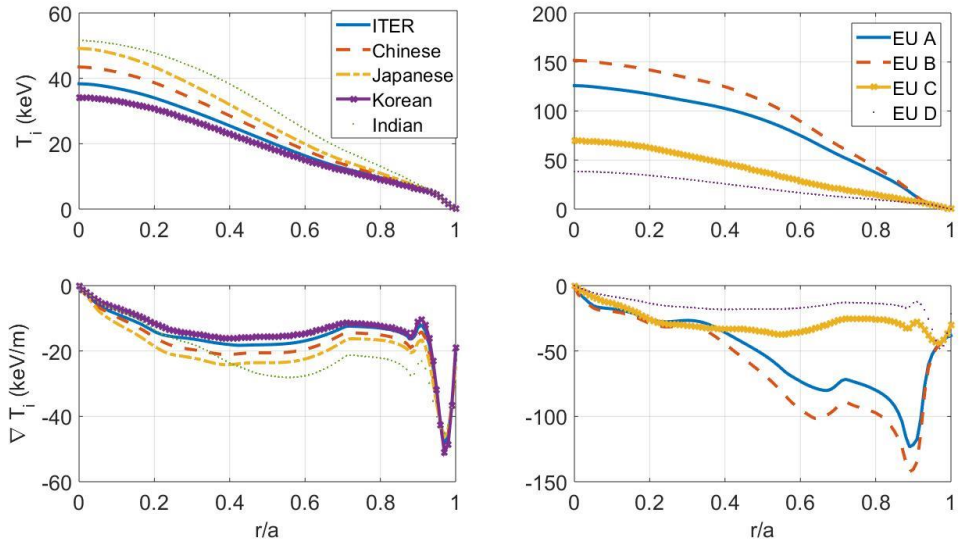

Figure 2. Ion temperature profiles (top panels) and ion temperature gradient profiles for the ITER and DEMOs (bottom panels) as a function of normalized minor radius.

debate. It is interesting for future work to revisit these results once an actual model is derived. Electron temperature profiles are not shown here but they yield similar results as those of ion temperature profiles. Their numerical values at plasma center can be seen in Table 2. For the central ion temperature, European model B yields the highest ion temperature, followed by model A, model C, Indian, Japanese, Chinese, European model D, ITER, and the Korean DEMO. For central electron temperature, European model B yields the highest value followed by model A, Indian, Japanese, European model C, model D, Chinese, ITER, and Korean. The orders are different because they depend on the heating schemes, plasma current, and effective charge.

Figure 3 illustrates ion and electron diffusivities profiles for the ITER and DEMOs. It is clear that their values drop close to the plasma center because only the neoclassical transports are dominant. The anomalous transport is driven by the local plasma temperature or pressure gradient so their values increase as the plasma gradients increase. Note, the differences in their values range by two orders of magnitude. Nevertheless, the diffusivities drop again at the plasma edge because the anomalous transport is quenched. This is another distinctive feature of ETB formation.

Table 2. Comparison of simulation results for ITER and DEMOs.

Device	$T_{i,0}$ (keV)	$T_{e,0}$ (keV)	P_α (MW)	W_{TOT} (T)	Q	τ (s)	f_{BS}
ITER	38.32	35.97	112	371	14	2.52	0.25
Chinese	43.46	36.16	107	378	7.23	2.30	0.26
Japanese	49.13	39.73	114	402	9.66	2.52	0.21
Korean	34.15	32.20	104	349	6.5	2.02	0.36
Indian	51.57	40.44	123	453	4.92	1.98	0.20
EU A	125.90	74.01	230	968	4.67	1.64	0.16
EU B	151.67	101.11	193	793	3.57	1.20	0.16
EU C	69.52	39.31	112	478	5	2.41	0.18
EU D	38.43	37.40	112	375	7.89	2.15	0.28

4.2 Electron density profiles

Figure 4 shows electron density and its gradient profiles as a function of normalized minor radius. The results agree with experimental measurements in which the density profiles are more flat than those of temperature profiles. This is because a part of the thermal sources is generated at the plasma core (alpha heating), whereas most of the density sources come from the edge of the plasma. The density sources that penetrate deeper into the plasma core are NBI and pellet injections. Pellet effects are not applied in this work, though it is possible that the pellet injection system will be installed in the ITER and DEMOs. ETB formation appears in the density channel as well. Experimentally, it is possible for an ETB to form only in a single channel or in both temperature and density channels simultaneously. Similar to the case of thermal diffusivities, the electron diffusivities are relatively low near the plasma center and increase toward the edge. Their values are reduced again in the ETB region.

4.3 Fusion power and performance comparisons

This section compares simulation results of the ITER and DEMOs as summarized numerically in Table 2. In the table, $T_{i,0}$ and $T_{e,0}$ are ion and electron temperatures at the plasma center, respectively, P_α represents alpha power, W_{TOT} represents total fusion power, and the fusion Q is a measure of plasma performance defined as:

$$Q \equiv \frac{5 \times P_\alpha}{P_{aux}} \tag{14}$$

which represents the ratio of total output power to input power, τ is the plasma confinement time, and f_{BS} is the bootstrap fraction. Overall, the European DEMO B yields the highest central ion and electron temperatures. The European

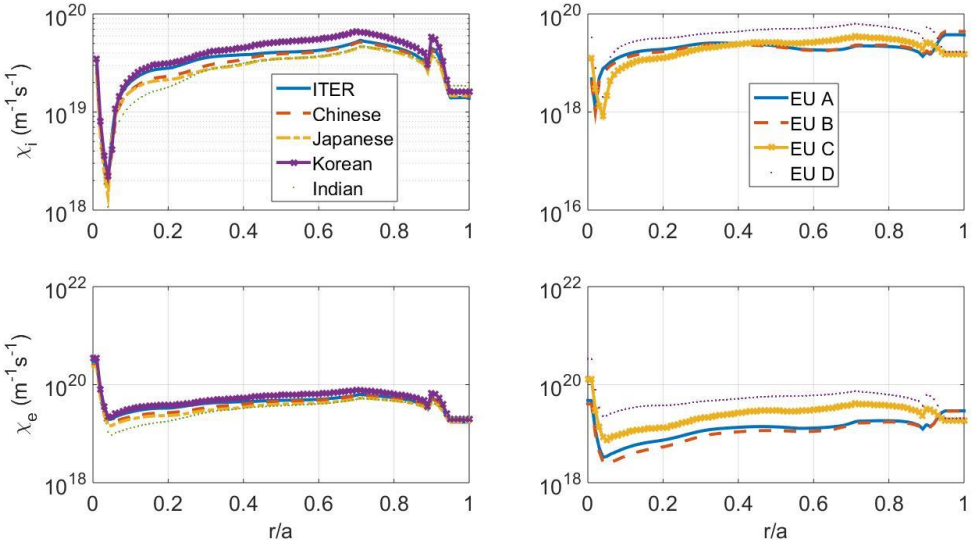

Figure 3. Semi-log plot of ion (top panels) and electron (bottom panels) diffusivities for the ITER and DEMOs as a function of normalized minor radius.

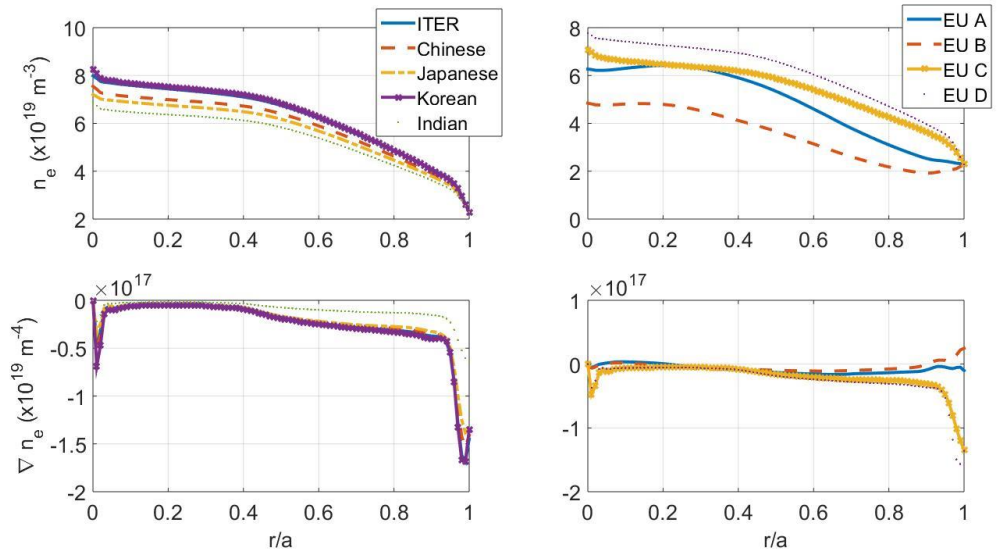

Figure 4. Electron density profiles (top panels) and electron density gradient profiles for the ITER and DEMOs (bottom panels) as a function of normalized minor radius.

DEMO A yields the highest alpha power and total fusion power. On the other hand, the Korean DEMO yields the least of those values. It appears that ITER produces the highest fusion Q because it provides the highest alpha heating while requiring the least amount of auxiliary power. The energy confinement time appears to also be the highest in the ITER and Japanese DEMO simulations. This is a quantity used to measure roughly how long plasma energy can be sustained if no heating is given. For a tokamak to be used as a fusion reactor, the confinement time of around a few seconds is required. From these data, all devices are applicable. Another interesting factor to be considered for a fusion power plant is the bootstrap current fraction. A tokamak is intrinsically a pulse machine because it requires an external transformer to produce inductive plasma current. This is not acceptable in a reactor because steady-state operation is desired. Fortunately, there are ways to provide non-inductive current drive for example NBI and lower hybrid heating can boost the current of the plasma. Bootstrap current is a self-generated current inside a plasma via the neoclassical effect. A higher bootstrap fraction implies a lower amount of external current drive is needed. The highest f_{BS} is found in the Korean DEMO and the lowest is found in the European DEMO models A and B.

5. Conclusions

Simulations of the ITER, Chinese, Japanese, Korean, Indian, and European DEMOs (model A, B, C, and D) in *H*-mode were carried out using CRONOS integrated predictive modelling code. The core transport is a combi-

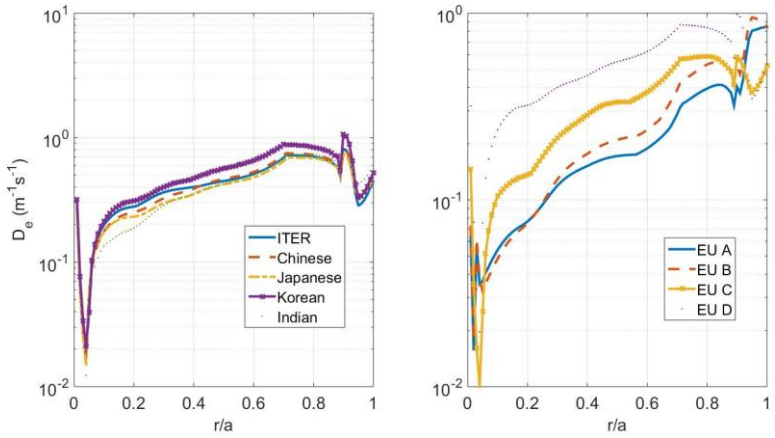

Figure 5. Semi-log plot of electron particle diffusivities for the ITER and DEMOs as a function of normalized minor radius.

nation of anomalous transport Mixed Bohm/gyro-Bohm, and the NCLASS module. The boundary condition of the transport solver is set at the top of the pedestal where its value is calculated based on empirical scaling. It is found that *H*-mode can be obtained in both ion and electron temperatures and electron density channels. Based on fusion *Q*, the ITER yielded the highest performance but the European DEMO B yielded the highest temperatures as well as fusion power output. The bootstrap fraction was the highest in the Korean DEMO at around 36%.

Acknowledgements

This work was partly supported by the government budget of Prince of Songkla University, project ID SCI61 0152S and the International Atomic Energy Agency (IAEA) under Contract No. 22785. The authors greatly thank J. Garcia and J.F. Artaud, IRFM, CEA for generous advice and consultation. This project is a part of a collaborative research under Center of Plasma and Nuclear Fusion Technology (CPaF).

References

Artaud, J. F., Basiuk, V., Imbeaux, F., Schneider, M., Garcia, J., Giruzzi, G., . . . Turco, F. (2010). The CRONOS suite of codes for integrated tokamak modelling. *Nuclear Fusion, 50*(4), 043001.

ASDEX Team (1989). The H-Mode of ASDEX. *Nuclear Fusion, 29*(11), 1959. doi:10.1088/0029-5515/29/11/010

Aymar, R., Barabaschi, P., & Shimomura, Y. (2002). The ITER design. *Plasma Physics and Controlled Fusion, 44*(5), 519. doi:10.1088/0741-3335/44/5/304

Basiuk, V., Artaud, J. F., Imbeaux, F., Litaudon, X., Bécoulet, A., Eriksson, L.-G., . . . Peysson, Y. (2003). Simulations of steady-state scenarios for Tore Supra using the CRONOS code. *Nuclear Fusion, 43*(9), 822.

Burrell, K. H. (1997). Effects of E x B velocity shear and magnetic shear on turbulence and transport in magnetic confinement devices. *Physics of Plasmas, 4*(5), 1499-1518. doi:10.1063/1.872367

Cenacchi, G., & Taroni, A. (1988). JETTO: A free boundary plasma transport code. *ENEA Report RT/TIB, 88*, 5.

Chatthong, B., & Onjun, T. (2013). Simulations of ITER in the presence of ITB using the NTV intrinsic toroidal rotation model. *Nuclear Fusion, 53*(1), 013007.

Chatthong, B., & Onjun, T. (2014). Comparison of H-mode plasma simulations using toroidal velocity models depending on plasma current density and ion temperature in presence of an ITB. *Songklanakarin Journal of Science and Technology, 36*(3), 375-387.

Chouli, B., Fenzi, C., Garbet, X., Bourdelle, C., Sarazin, Y., Rice, J., . . . the Tore Supra Team. (2015). Investigations of LHCD induced plasma rotation in Tore Supra. *Plasma Physics and Controlled Fusion, 57*(12), 125007.

Dale, M. (2010). 50 years of fusion research. *Nuclear Fusion, 50*(1), 014004.

Deng, Z., John, H. S., Yemin, H., Guoqiang, L., Qilong, R., & Jin, O. (2009). Transport Modelling for EAST with LHRF and NBI. *Plasma Science and Technology, 11*(4), 417.

Erba, M., Aniel, T., Basiuk, V., Becoulet, A., & Litaudon, X. (1998). Validation of a new mixed Bohm/gyro-Bohm model for electron and ion heat transport against the ITER, Tore Supra and START database discharges. *Nuclear Fusion, 38*(7), 1013.

Erba, M., Parail, V., Springmann, E., & Taroni, A. (1995). Extension of a Bohm model for L-mode electron heat transport to ion heat transport and to the ohmic regime. *Plasma Physics and Controlled Fusion, 37*(11), 1249.

Feng, K. M., Zhang, G. S., Zheng, G. Y., Zhao, Z., Yuan, T., Li, Z. Q., . . . Pan, C. H. (2009). Conceptual design study of fusion DEMO plant at SWIP. *Fusion Engineering and Design, 84*(12), 2109-2113. doi:10.1016/j.fusengdes.2009.01.104

Hinton, F. L., & Hazeltine, R. D. (1976). Theory of plasma transport in toroidal confinement systems. *Reviews of Modern Physics, 48*(Copyright (C) 2010 The American Physical Society), 239.

Honda, M., & Fukuyama, A. (2008). Dynamic transport simulation code including plasma rotation and radial

electric field. *Journal of Computational Physics, 227*(5), 2808-2844. doi:10.1016/j.jcp.2007.11.017

Houlberg, W. A., Shaing, K. C., Hirshman, S. P., & Zarnstorff, M. C. (1997). Bootstrap current and neoclassical transport in tokamaks of arbitrary collisionality and aspect ratio. *Physics of Plasmas, 4*(9), 3230-3242.

Hubbard, A. E. (2000). Physics and scaling of the H-mode pedestal. *Plasma Physics and Controlled Fusion, 42*(5A), A15.

Jardin, S. C., Pomphrey, N., & DeLucia, J. (1986). Dynamic modeling of transport and positional control of tokamaks. *Journal of Computational Physics, 66*(2), 481.

Kessel, C. E., Giruzzi, G., Sips, A. C. C., Budny, R. V., Artaud, J. F., Basiuk, V., . . . Tucillo, A. A. (2007). Simulation of the hybrid and steady state advanced operating modes in ITER. *Nuclear Fusion, 47*(9), 1274.

Kim, K., Im, K., Kim, H. C., Oh, S., Park, J. S., Kwon, S., . . . Zhai, Y. (2015). Design concept of K-DEMO for near-term implementation. *Nuclear Fusion, 55*(5), 053027.

Kim, S. H., Artaud, J. F., Basiuk, V., Bécoulet, A., Dokuka, V., Hoang, G. T., . . . Lukash, V. E. (2009). Lower hybrid assisted plasma current ramp-up in ITER. *Plasma Physics and Controlled Fusion, 51*(6), 065020.

Kinsey, J. E., Staebler, G. M., & Waltz, R. E. (2002). Simulations of internal transport barrier formation in tokamak discharges using the GLF23 transport model. *Physics of Plasmas, 9*(5), 1676-1691.

Maisonnier, D., Cook, I., Pierre, S., Lorenzo, B., Luigi, D. P., Luciano, G., . . . Aldo, P. (2006). DEMO and fusion power plant conceptual studies in Europe. *Fusion Engineering and Design, 81*(8–14), 1123-1130. doi:10.1016/j.fusengdes.2005.08.055

Pearlstein, L. D., Bulmer, R. H., Casper, T. A., Hooper, E. B., Jong, R. A., Kaiser, T. B., & LoDestro, L. L. (2001). Predictive modelling of axisymmetric toroidal configurations. *ECA, 25A*, 1901-1904.

Pereverzev, G., & Yushmanov, P. N. (2002). ASTRA automated system for transport analysis in a Tokamak. *Max-Planck Institut fur Plasmaphysik*, IPP 5/98.

Righi E. the ITER H-mode Threshold Database Working Group (1998). Scaling of the H-mode power threshold for ITER. *Plasma Physics and Controlled Fusion, 40*(5), 857.

Singer, C. E., Post, D. E., Mikkelsen, D. R., Redi, M. H., McKenney, A., Silverman, A., . . . Ogden, J. (1988). Baldur: A one-dimensional plasma transport code. *Computer Physics Communications, 49*(2), 275-398. doi:10.1016/0010-4655(88)90012-4

Snipes, J. A., the international H-mode Threshold Database Working Group. (2000). Latest results on the H-mode threshold using the international H-mode threshold database. *Plasma Physics and Controlled Fusion, 42*(5A), A299.

Srinivasan, R., & Deshpande, S. P. (2008). Strategy for the Indian DEMO design. *Fusion Engineering and Design, 83*(7–9), 889-892. doi:10.1016/j.fusengdes.2008.07.038

Taroni, A., Erba, M., Springmann, E., & Tibone, F. (1994). Global and local energy confinement properties of simple transport coefficients of the Bohm type. *Plasma Physics and Controlled Fusion, 36*(10), 1629.

Tobita, K., Nishio, S., Enoeda, M., Sato, M., Isono, T., Sakurai, S., . . . Tsuru, D. (2006). Design study of fusion DEMO plant at JAERI. *Fusion Engineering and Design, 81*(8–14), 1151-1158. doi:10.1016/j.fusengdes.2005.08.058

Wagner, F. (2007). A quarter-century of H-mode studies. *Plasma Physics and Controlled Fusion, 49*(12B), B1. doi:10.1088/0741-3335/49/12b/s01

Wagner, F., Becker, G., Behringer, K., Campbell, D., Eberhagen, A., Engelhardt, W., . . . Röhr, H. (1982). Regime of improved confinement and high beta in neutral-beam-heated divertor discharges of the ASDEX Tokamak. *Physical Review Letters, 49*, 1408. doi:10.1103/physrevlett.49.1408